British Journal of Pharmacology (2009), 156, 432–443

0007-1188/09
www.brjpharmacol.org

RESEARCH PAPER

Accelerated inactivation of cardiac L-type calcium channels triggered by anaesthetic-induced preconditioning

A Tampo[1,4], CS Hogan[1], F Sedlic[1,2], ZJ Bosnjak[1,2] and WM Kwok[1,3]

[1]*Department of Anesthesiology, Medical College of Wisconsin, Milwaukee, WI, USA,* [2]*Department of Physiology, Medical College of Wisconsin, Milwaukee, WI, USA,* [3]*Department of Pharmacology and Toxicology, Medical College of Wisconsin, Milwaukee, WI, USA, and* [4]*Department of Anesthesiology and Critical Care Medicine, Asahikawa Medical College, Asahikawa, Japan*

Background and purpose: Cardioprotection against ischaemia by anaesthetic-induced preconditioning (APC) is well established. However, the mechanism underlying Ca^{2+} overload attenuation by APC is unknown. The effects of APC by isoflurane on the cardiac L-type Ca channel were investigated.
Experimental approach: In a model of *in vivo* APC, Wistar rats were exposed to isoflurane (1.4%), delivered via a vaporizer in an enclosure, prior to thoracotomy. The Dahl S rats were similarly preconditioned to determine strain-dependent effects. Whole-cell patch clamp using cardiac ventricular myocytes was used to determine the L-type Ca^{2+} current ($I_{Ca,L}$) characteristics and calmodulin (CaM) levels were determined by Western blot analysis. Cytosolic Ca^{2+} levels were monitored using fluo-4-AM. Action potential (AP) simulations examined the effects of APC.
Key results: In Wistar rats, APC significantly accelerated $I_{Ca,L}$ inactivation kinetics. This was abolished when external Ca^{2+} was replaced with Ba^{2+}, suggesting that Ca^{2+}-dependent inactivation of $I_{Ca,L}$ was modulated by APC. Expression levels of CaM, a determinant of $I_{Ca,L}$ inactivation, were not affected. Attenuation of cytosolic Ca^{2+} accumulation following oxidative stress was observed in the APC group. Simulations showed that the accelerated inactivation of $I_{Ca,L}$ resulted in a shortening of the AP duration. The Dahl S rat strain was resistant to APC and changes in $I_{Ca,L}$ inactivation were not observed in cardiomyocytes prepared from these rats.
Conclusions and implications: APC triggered persistent changes in the inactivation of cardiac L-type Ca channels. This can potentially lead to a reduction in Ca^{2+} influx and attenuation of Ca^{2+} overload during ischaemia/reperfusion.
British Journal of Pharmacology (2009) **156**, 432–443; doi:10.1111/j.1476-5381.2008.00026.x; published online 19 January 2009

Keywords: anaesthetic-induced preconditioning; cardioprotection; L-type calcium channel; volatile anaesthetics; isoflurane

Abbreviations: AP, action potential; APC, anaesthetic-induced preconditioning; APD, action potential duration; CaM, calmodulin; $I_{Ca,L}$, L-type calcium current; IPC, ischemic preconditioning; τ, time constant

Introduction

Ischemic preconditioning (IPC) confers cardioprotective effects whereby short, non-lethal ischemic episodes result in a significant reduction in infarct size following a subsequent prolonged ischaemia (Murry *et al.*, 1986). Since IPC is invoked by a short, non-fatal ischemic period, its potential clinical application may be limited due to the difficulty in precisely timing the preconditioning ischemic stimulus. However, several pharmacological agents including volatile anaesthetics are known to mimic the cardioprotective effects of IPC (Cason *et al.*, 1997; Kersten *et al.*, 1997a). The efficacy of anaesthetic-induced preconditioning (APC) is similar to that of IPC, and mechanisms underlying its cardioprotective effects have been intensely investigated. The key components of the intracellular signal transduction pathways include G-proteins, protein kinase C (PKC)-δ and ε isoforms, protein tyrosine kinase, mitogen-activated protein kinase, reactive oxygen species, sarcolemmal and mitochondrial ATP-sensitive potassium channels (sarcK_{ATP} and mitoK_{ATP} channels respectively) (Kersten *et al.*, 1997b; Tanaka *et al.*, 2002; Zaugg *et al.*, 2002; Ludwig *et al.*, 2004; da Silva *et al.*, 2004; Marinovic *et al.*, 2006). Recent evidence suggests that the signalling pathways converge at the mitochondria and preserve their function, resulting in

Correspondence: Dr Wai-Meng Kwok, Department of Anesthesiology, Medical College of Wisconsin, 8701 Watertown Plank Road, Milwaukee, WI 53226, USA.
E-mail: wmkwok@mcw.edu
Received 20 June 2008; revised 29 August 2008; accepted 8 September 2008

the cardioprotective effects afforded by preconditioning (Krolikowski *et al.*, 2005; Riess *et al.*, 2005; Ljubkovic *et al.*, 2007). Nevertheless, key questions still remain unanswered on how the converging signalling cascades affect mitochondrial function and ultimately lead to cardioprotection.

In addition, whether there is a genetic component to APC has not been clearly established. Previous studies have reported species-dependent differences in response to myocardial ischaemia (Galinanes and Hearse, 1990). Furthermore, differential responses to resistance to myocardial ischaemia have been shown in different rat strains (Baker *et al.*, 2000). Thus, a genetic component may also underlie the efficacy of cardioprotection by APC.

A physiologically beneficial outcome of APC that confers cardioprotection appears to be the attenuation of Ca^{2+} overload following ischaemia/reperfusion (Hoka *et al.*, 1987; An *et al.*, 2001; Varadarajan *et al.*, 2002). However, the mechanism underlying this attenuation is unknown. A major source of myocardial Ca^{2+} entry is via the L-type Ca channel. Consequently, inhibition of the L-type Ca channel can result in reduced Ca^{2+} entry, and thus lead to diminished Ca^{2+} overload. On the other hand, Ca^{2+} entry via the L-type Ca channel may also contribute to preconditioning. A small increase in intracellular Ca^{2+} during IPC or Ca^{2+} preconditioning has been reported to trigger PKC-dependent pathways that contributed to the induction of cardioprotection (Miyawaki and Ashraf, 1997). This was abolished by blockade of Ca^{2+} influx via the reverse mode of the Na^+/Ca^{2+} exchanger and the L-type Ca channel. Furthermore, atrial trabeculae extracted from patients taking L-type Ca channel blockers were resistant to cardioprotection by IPC (Cain *et al.*, 1999). Though an increase in cytosolic Ca^{2+} by IPC would appear to counteract its cardioprotective effect, a rise in cytosolic Ca^{2+} during an initial episode of brief ischaemia can become attenuated in subsequent episodes of ischaemia (Smith *et al.*, 1996). Thus, a transient ischaemic event can lead to a rapid adaptation of Ca^{2+} homeostasis during subsequent episodes.

Based on these previous reports, the L-type Ca channel may potentially play diverse but pivotal functional roles in protecting the myocardium during preconditioning. Ca^{2+} influx may contribute to the underlying cardioprotective signalling cascade, while its attenuation may contribute to a reduction in reperfusion injury. The consequence of a preconditioning stimulus on this channel has not been established. Furthermore, whether APC affects the molecular modulators of Ca channel function has not been investigated. For example, the effect of APC on CaM is unknown even though a major aspect of Ca^{2+}-dependent inactivation is the involvement of CaM, through its association with the channel (Dick *et al.*, 2008).

The purpose of this study was to investigate the effect of preconditioning on the cardiac L-type Ca channel current, $I_{Ca,L}$. We hypothesized that preconditioning triggers persistent changes in the biophysical profile of the L-type Ca channel and a physiologically relevant model of *in vivo* APC with isoflurane was utilized to test this hypothesis. Our results showed that APC triggered a persistent change in the inactivation profile of the L-type Ca channel, with a specific acceleration of Ca^{2+}-dependent inactivation.

Methods

In vivo *anaesthetic-induced preconditioning*

This study was approved by the Institutional Animal Care and Use Committee of the Medical College of Wisconsin. Adult male Wistar and Dahl S rats (Harlan, Indianapolis, IN) were used for this study. Two strains of rats were chosen to determine whether the efficacy of APC was dependent on strain, which would be indicative of a genetic component. The rats were divided into two groups, non-APC (control) and APC (*in vivo* preconditioning). For *in vivo* APC, rats were exposed to 1.4% (1.0 minimum alveolar concentration) isoflurane (Baxter, Deerfield, IL) delivered via a vaporizer in an enclosure for 30 min followed by a 30 min recovery period prior to thoracotomy (Stadnicka *et al.*, 2006). In the non-APC group, rats were not exposed to isoflurane prior to thoracotomy. This was a physiologically relevant model of preconditioning by APC. Since the rats were exposed to isoflurane in an enclosure, the animals were subjected to all the triggering events induced by the volatile anaesthetic and not only to those confined to the heart. This included any changes in the systemic input and contributions from the vasculature and the endothelium. This contrasts with the method of preconditioning using an isolated heart on a Langendorff apparatus where the preconditioning stimulus is applied at the level of the organ, in the absence of systemic input.

Isolation of cardiac ventricular myocytes

Cardiac ventricular myocytes were enzymatically isolated from adult male Wistar and Dahl S rats weighing 180–280 g as previously described (Aizawa *et al.*, 2004). Briefly, rats were anaesthetized with thiobutabarbital (Inactin, 200 $mg \cdot kg^{-1}$, i.p.) and heparinized with 1000 U heparin (Baxter). Under anaesthesia, the heart was quickly removed and mounted on a Langendorff apparatus followed by retrograde perfusion through the aorta with a solution containing Joklik medium (Sigma-Aldrich, St. Louis, MO) and heparin at pH 7.23. After allowing for the blood to clear from the heart (for approximately 1–2 min), the perfusate was replaced with an enzyme solution containing Joklik medium, collagenase (Type II; Invitrogen, Carlsberg, CA), protease (Type XIV) and bovine serum albumin (Serologicals Proteins, Kankakee, IL) at pH 7.23. The solutions were gassed with 95% O_2 and 5% CO_2, and the temperature was maintained at 37°C. Following 15–20 min of perfusion with the enzyme solution, the ventricles were cut from the heart, minced and incubated in a shaking bath with the enzyme solution for 5–8 min. The resulting myocyte suspension was then filtered, centrifuged and stored in a modified Tyrode solution at room temperature. The myocytes were used for experiments within 10 h following the isolation procedure.

Solutions

The isolated cardiomyocytes were stored in a modified Tyrode solution that contained (in $mmol \cdot L^{-1}$): 132 NaCl, 4.8 KCl, 1 $CaCl_2$, 1.2 $MgCl_2$, 10 HEPES, 5 dextrose, and pH was adjusted to 7.4 with NaOH. For the recording of whole-cell $I_{Ca,L}$, the

pipette solution contained (in mmol·L^{-1}): 110 CsCl (substitute for potassium), 1 $CaCl_2$, 1 $MgCl_2$, 11 EGTA, 10 HEPES, 5 Mg-ATP, at pH 7.3 adjusted with CsOH. To isolate for $I_{Ca,L}$, the bath (external) solution contained (in mmol·L^{-1}): 132 N-methyl-D-glucamine (substitute for sodium), 4.8 CsCl, 2 $CaCl_2$, 2 $MgCl_2$, 10 HEPES, 5 dextrose and 5 mmol·L^{-1} of 4-aminopyridine (transient outward potassium current antagonist), at pH 7.4 adjusted with HCl. For the investigation of the voltage-dependent inactivation and recovery from slow inactivation, $CaCl_2$ was replaced with $BaCl_2$, so Ba^{2+} was the charge carrier to remove Ca^{2+}-dependent inactivation. All chemicals used in this study were obtained from Sigma-Aldrich (St. Louis, MO), unless otherwise noted.

Oxidative stress

A cell survival study was conducted to validate the *in vivo* APC model by comparing the tolerance against oxidative stress between the non-APC and APC myocytes (Marinovic *et al*., 2006). The cell suspension was transferred to a chamber on an inverted microscope (Eclipse TE2000-U; Nikon, Tokyo, Japan) and the myocytes were allowed to settle for 10 min, after which they eventually attached to the glass coverslip. They were then exposed to 0.4% Trypan blue solution for 2 min followed by washout with glucose-free Tyrode solution. Cells that were rod-shaped and not stained were considered to be viable and this number was counted. Following a 5 min perfusion with the glucose-free Tyrode solution, the myocytes were subjected to oxidative stress by perfusion with 200 μmol·L^{-1} H_2O_2 and 100 μmol·L^{-1} $FeSO_4$ for 17 min. Subsequently, the myocytes were reperfused with glucose-free Tyrode solution for another 20 min. The myocytes were exposed to Trypan blue again and the living myocytes were counted to determine the percentage of cell death. For each group, 3–4 rats were utilized, and 1–3 experiments were conducted from myocytes isolated from each animal. The percentage of cell death was calculated from at least 200 myocytes for each experiment. For the survival study, the *n* number denotes the number of experiments that were conducted.

Electrophysiology

The whole-cell configuration of the patch clamp technique was used to record $I_{Ca,L}$. Patch pipettes were pulled from borosilicate glass capillary tubes (Garner Glass, Claremont, CA) using a horizontal micropipette puller (P-97; Sutter Instrument, Novato, CA), and heat polished using a microforge (MF-830; Narishige, Tokyo, Japan). The pipette resistances were in the range of 2–5 MΩ. $I_{Ca,L}$ was monitored using a patch clamp amplifier (Axopatch 200B; Molecular Devices, Sunnyvale, CA) interfaced with a digitizer (Digidata 1322A; Molecular Devices) to a computer. Data acquisition and analysis were conducted using pClamp 9.2 (Molecular Devices), and additional analyses were performed using Origin 7 (OriginLab, Northampton, MA). All the experiments were performed under room temperature. For the patch clamp studies, 38 rats were utilized (19 each for the non-APC and APC groups). The *n* number denotes the number of myocytes from which the current recordings were obtained.

L-type Ca^{2+} current measurement

$I_{Ca,L}$ was elicited by 400 ms duration test pulses from a holding potential of –80 to +50 mV in 10 mV increments at a rate of 0.33 Hz. A conditioning pulse (to –50 mV; 50 ms) was used to inactivate any residual cardiac sodium current before each test pulse. $I_{Ca,L}$ was normalized to cell capacitance and the resultant current density was plotted against the test potentials to yield the current-voltage relationship.

Steady-state activation curve

The conductance was calculated with the following equation, $G = I/(V_m - V_{rev})$, where I is the current amplitude, V_m is the test potential and V_{rev} is the reversal potential. The corresponding steady-state activation curves were obtained by normalizing the conductance to the peak conductance. The normalized conductances (G/G_{max}) were then plotted against the test potentials and fitted with the Boltzmann function,

$$G/G_{max} = 1/1 + \exp[-(V_m - V_{1/2})/k]$$

where $V_{1/2}$ is the voltage at half-maximal conductance and k is the slope factor.

Steady-state inactivation curve

The steady-state inactivation curves were obtained using a standard protocol, in which 500 ms conditioning pulses from a holding potential of –80 mV to +20 mV in 10 mV increments were followed by a 600 ms test pulse to 0 mV. Current amplitude was normalized to the peak current (I/I_{max}), and plotted against each conditioning potential. The steady-state inactivation curves were also fitted with the Boltzmann function,

$$I/I_{max} = 1/1 + \exp[(V_m - V_{1/2})/k]$$

to obtain $V_{1/2}$, the voltage at which half the channels are available for opening, and k, the slope factor.

Recovery from fast and slow inactivation

A standard two-pulse protocol was used to monitor the recovery of $I_{Ca,L}$ from fast inactivation. A 500 ms conditioning pulse to 0 mV was followed by a 600 ms test pulse to 0 mV in varying intervals from 0 to 550 ms in 50 ms increments. The holding potential was set at –80 mV. Current amplitude elicited by the test pulses were normalized to the peak current elicited by the conditioning pulse. The normalized currents were plotted against each time interval, and fitted with a single exponential function that yielded the time constant for recovery from fast inactivation.

To investigate the recovery from slow inactivation, Ba^{2+} was used as the charge carrier. The Ba^{2+} current, I_{Ba}, was elicited using a two-pulse protocol, in which a 5 s conditioning pulse to 0 mV was followed by a 50 ms test pulse to 0 mV in varying intervals from 1 to 15 s in 1 s increments from a holding potential of –80 mV. Current amplitude obtained during the test pulse was normalized to the peak current obtained during the conditioning pulse and plotted against the varying time intervals. The resultant plot was then fitted with a double

exponential function to obtain the fast and slow time constants (τ_{fast} and τ_{slow} respectively) for the recovery from slow inactivation.

Ca^{2+} current inactivation kinetics and transmembrane charge transfer

$I_{Ca,L}$ inactivation kinetics were quantified by fitting the current traces with a double exponential function of the form

$$I_{Ca,L} = A_{fast} \times \exp(-t/\tau_{fast}) + A_{slow} \times \exp(-t/\tau_{slow}) + C$$

where τ_{fast} and τ_{slow} are the fast and slow time constants, respectively, A_{fast} and A_{slow} are the respective amplitudes of the time constants, and C is the final amplitude following the inactivation. The fraction of channels that gated either fast or slow was quantified by the respective amplitudes with the following equations:

$$Fraction_{slow} = A_{slow}/(A_{fast} + A_{slow})$$

$$Fraction_{fast} = A_{fast}/(A_{fast} + A_{slow})$$

In experiments where the voltage-dependent inactivation of $I_{Ca,L}$ was investigated, Ba^{2+} substituted for Ca^{2+} as the charge carrier in the external solution to remove Ca^{2+}-dependent inactivation and the Ba^{2+} current (I_{Ba}) was recorded.

To correlate the changes in Ca^{2+} influx to the changes in $I_{Ca,L}$ inactivation kinetics, the transmembrane charge transfer was determined. This was calculated by integrating the area of $I_{Ca,L}$ traces after the capacitive transients to the time point of 100 ms. This temporal duration was chosen to mimic the time course of a rat action potential at room temperature (Linz and Meyer, 2000).

Western blotting

Western blot analysis was carried out to determine the cytosolic levels of calmodulin (CaM). Ventricles were excised from both non-APC and APC hearts, and homogenized on ice in a solution that contained (in mmol·L^{-1}): 20 Tris-HCl, 150 NaCl, 1 EDTA, 1 EGTA, 1% Triton X-100, and cocktails of protease inhibitors (complete mini; Roche, Indianapolis, IN) and phosphatase inhibitors (cocktail set II; Calbiochem, San Diego, CA), pH 7.4. The homogenate was centrifuged for 10 min at 10 000× *g* (4°C), and the resulting supernatant was centrifuged for 1 h at 100 000× *g* (4°C) to separate the cytosolic and membrane fractions. The total protein concentration was determined by a modified Lowry method (Bio-Rad, Hercules, CA). Equal amounts of proteins (100 μg) were separated on a 15% polyacrylamide gel and transferred to the nitrocellulose membrane (Bio-Rad). The membrane was blocked with 5% fat-free milk and incubated overnight at 4°C with a rabbit monoclonal CaM antibody (Epitomics, Burlingame, CA) at 1:1000 dilution. After being washed, the membrane was incubated for 1 h at room temperature with a horseradish peroxidase-conjugated anti-rabbit immunoglobulin G (Bio-Rad) at 1:10 000 dilution. Chemiluminescence was detected after incubation with Luminol/Enhancer solution (Pierce, Rockford, IL) using radiographic film. To verify equal protein loading, the membrane was re-probed with a mouse monoclonal anti-β-actin antibody at 1:1000 dilution followed by incubation with a horseradish peroxidase-conjugated anti-mouse immunoglobulin G (Bio-Rad) at 1:5000 dilution and developed on film. CaM/β-actin ratio was quantified using the ImageJ software (National Institutes of Health, Bethesda, MD).

Cytosolic Ca^{2+} measurement

A Ca^{2+}-sensitive indicator, fluo-4-AM (2 μmol·L^{-1}; Invitrogen, Carlsbad, CA) that preferentially loaded into the cytosol was used to assess cytosolic Ca^{2+}. Images were obtained with a confocal microscope (Eclipse TE2000-U) equipped with a 40×/1.3 oil-immersion objective. Excitation at 488 nm was achieved with an argon laser. After 20 min of dye loading, followed by a 5 min dye washout, cells were exposed to an oxidative stress protocol identical to that used in the cell survival study described above. Images were taken every 5 min. Data were analysed with the Metamorph 6.1 software (Universal Imaging, West Chester, PA).

Simulation of the action potential

Simulations of the cardiac AP were conducted using Cellular Open Resource (COR), a modelling environment developed by the Oxford Cardiac Electrophysiology Group in the Department of Physiology at the University of Oxford (Great Britain) (Garny *et al.*, 2003). Specifically, simulations were run using the Fox-McHarg-Gilmour (FMG) model on COR (Fox *et al.*, 2002). This model was chosen for its ease of use in determining the effect of changes in the L-type Ca channel's Ca^{2+}-dependent inactivation on the AP profile. To simulate an AP with the time course that mimicked that of a rat cardiac AP at room temperature, the FMG model was modified by adjusting the amplitudes of the following potassium (K) currents: I_{to} (transient outward K current), I_{Kr} (rapidly activating delayed rectifier K current), I_{Kp} (plateau K current) and I_{K1} (inward rectifier K current). Contributions from I_{Ks} (slowly activating delayed rectifier K current) were eliminated. In addition, since the original FMG model included an enhanced Ca^{2+}-dependent inactivation of the L-type Ca channel, modifications were made to incorporate the 'basal' rate of Ca^{2+}-dependent inactivation as described by the phase-2 Luo-Rudy model (Luo and Rudy, 1994). Specifically, the Ca^{2+}-dependent inactivation gate at steady state was defined by

$$f_{Ca} = 1/\left[1 + ([Ca^{2+}]_i/K_{mfCa})^2\right]$$

where $[Ca^{2+}]_i$ is the intracellular Ca^{2+} concentration, and K_{mfCa} is the half-saturation constant. For the initial conditions, K_{mfCa} was set at 0.60 μmol·L^{-1} (Luo and Rudy, 1994).

Statistical analysis

Data are shown as mean ± SEM. One-way ANOVA followed by Scheffe's test was used to compare the data among the three groups in the cell survival study. The unpaired Student's *t*-test was used for comparisons between the non-APC and APC groups in the patch clamp studies and Ca^{2+} measure-

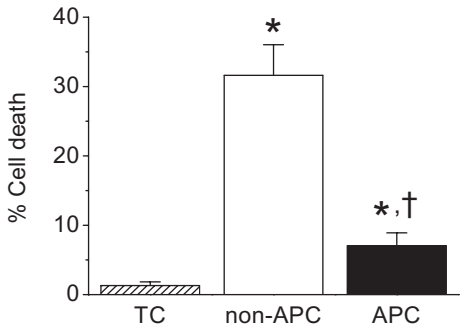

Figure 1 Effects of *in vivo* APC on cardiomyocyte survival after oxidative stress. Myocytes were isolated from Wistar rat hearts. In the non-APC group, oxidative stress significantly increased the percentage of cell death compared with the time control (TC) group. This effect of oxidative stress was significantly attenuated by *in vivo* APC. *$P < 0.05$ vs. TC, †$P < 0.05$ vs. non-APC. $n = 7$–10 per group.

ments. Statistical analyses were performed using the Origin 7 software and $P < 0.05$ was considered significantly different.

Results

Validation of the in vivo *APC model: protection against oxidative stress*

To validate the effectiveness of the *in vivo* APC model, a cell survival study was conducted to determine the efficacy of *in vivo* APC in inducing tolerance against oxidative stress injury on isolated myocytes obtained from the Wistar rats. Myocytes from the non-APC and APC groups were subjected to oxidative stress as described in *Methods*. As a time control, myocytes were perfused for 42 min with glucose-free Tyrode solution. As shown in Figure 1, in the time control group, the per cent cell death was low after this perfusion. In the non-APC group, oxidative stress resulted in a markedly increased proportion of dead cells and exposure to the APC protocol significantly attenuated this high percentage of cell death in myocytes following oxidative stress. These results using the Wistar rats confirmed that *in vivo* APC was very effective in decreasing cell death following oxidative stress. This cardioprotection persisted past the cell isolation procedure.

Effects of in vivo *APC on $I_{Ca,L}$ steady-state activation, inactivation and recovery from inactivation*

To characterize the effects of APC on $I_{Ca,L}$, whole-cell current recordings were made from isolated myocytes obtained from Wistar rats that had been previously preconditioned by isoflurane via the *in vivo* APC protocol. The $I_{Ca,L}$ current-voltage relationship, the steady-state activation and inactivation curves, and the recovery from fast and slow inactivation were determined. Figure 2A depicts representative $I_{Ca,L}$ traces recorded from ventricular myocytes isolated from a control (non-APC) rat heart. The current-voltage relationships obtained from the non-APC and APC groups suggested that the voltage dependence of activation was unaltered by APC (Figure 2B). The peak $I_{Ca,L}$ densities were also not significantly different between the two groups with -7.6 ± 0.4 pA·pF^{-1} in the non-APC and -8.8 ± 0.5 pA·pF^{-1} in the APC groups ($n = 21$–22 per group). The absence of a significant shift in the voltage dependence of activation was confirmed by constructing the steady-state activation curve (Figure 2C, Table 1). In addition, the steady-state inactivation curves obtained from the non-APC and APC groups were not significantly different (Figure 2D, Table 1). Moreover, recovery from fast inactivation of $I_{Ca,L}$ was not affected by *in vivo* APC (Figure 2E, Table 1). As $I_{Ca,L}$ also exhibits slow inactivation, the effect of APC on recovery from slow inactivation was determined. As was the case for recovery from fast inactivation, APC had no significant effect on recovery from slow inactivation (Figure 2F, Table 1).

Effects of in vivo *APC on $I_{Ca,L}$ inactivation kinetics and transmembrane charge transfer*

Though *in vivo* APC did not result in any significant persistent changes in the steady-state activation and inactivation curves, and in the recovery from fast and slow inactivation, it did significantly accelerate $I_{Ca,L}$ inactivation kinetics, as demonstrated in Figure 3A. Specifically, τ_{fast} in the voltage range of –20 to +10 mV, and τ_{slow} in the voltage range from –20 to +40 mV were significantly decreased compared with the non-APC group ($n = 21$–22 per group; Figure 3B). Additional analysis of $I_{Ca,L}$ inactivation, fitted with the double exponential function (see *Methods*), revealed that APC induced a greater fraction of channels to favour fast inactivation as determined by the relative fraction of channels that gated fast (Figure 3c). This was accompanied by a corresponding decrease in the relative fraction of channels that gated slow (data not shown). These results were not affected by the time interval between cell isolation and the electrophysiological recordings, and persisted during the 10 h period the myocytes were used.

In order to quantify the change in ionic influx due to the acceleration of $I_{Ca,L}$ inactivation, the transmembrane charge transfer was determined. To correlate Ca^{2+} influx during a rat ventricular AP, the charge transfer was calculated during 100 ms. As summarized in Figure 3D, a significant decrease in charge transfer resulted from the APC-triggered acceleration of $I_{Ca,L}$ inactivation.

As the inactivation of $I_{Ca,L}$ consists of voltage- and Ca^{2+}-dependent components, experiments were conducted to determine which of the components, if not both, were affected by APC. The result above showed an increase in the fraction of channels in the fast inactivated state, which suggested that the effect of APC was likely to be on the Ca^{2+}-dependent inactivation of the channel. Consequently, experiments were conducted to test this hypothesis. Ba^{2+} was utilized as the charge carrier to remove Ca^{2+}-dependent inactivation. Under this condition, the inactivation of $I_{Ca,L}$ was due to the voltage-dependent mechanism. As shown in Figure 4A, I_{Ba} exhibited markedly slower inactivation kinetics as expected. In contrast to its effect on $I_{Ca,L}$, APC did not affect I_{Ba} inactivation kinetics (Figure 4B). Under our recording conditions, inactivation of I_{Ba} was best fitted by a double exponential function (Findlay, 2002). This indicated that APC accelerated the Ca^{2+}-dependent inactivation of $I_{Ca,L}$, but had no effect on voltage-dependent inactivation.

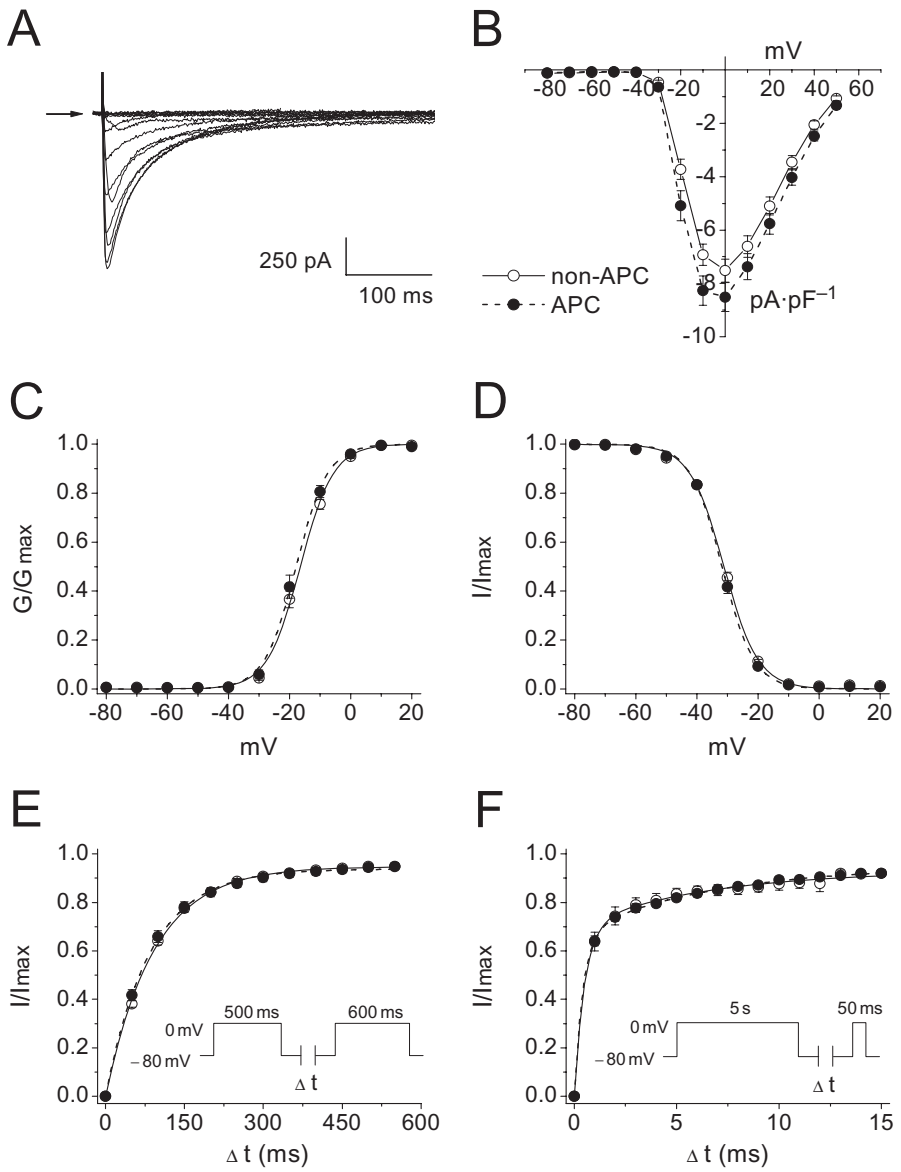

Figure 2 Effects of *in vivo* APC on the biophysical profile of $I_{Ca,L}$ obtained in myocytes from non-APC and APC hearts. (A) Representative whole-cell $I_{Ca,L}$ recorded from an isolated cardiomyocyte obtained from a non-APC heart. Arrow indicates zero current level. (B) Current-voltage relationship. The current-voltage relationship for the non-APC and APC groups are shown. No significant differences were observed (n = 21–22 per group). (C) Steady-state activation curves. Data were fitted with the Boltzmann function. No significant shifts in the steady-state activation curves were observed between the two groups (n = 21–22 per group). (D) Steady-state inactivation curves. Similarly to (C), data were fitted with the Boltzmann function. No significant shifts in the steady-state inactivation curves were observed between the two groups (n = 22 per group). (E) Recovery from fast inactivation. The inset depicts the standard two-pulse protocol that was utilized as described in *Methods* (n = 19 per group). (F) Recovery from slow inactivation. The inset depicts the two pulse protocol that was utilized as described in *Methods* (n = 4 per group). There were no significant differences in the recoveries from fast and slow inactivations between the non-APC and APC groups.

Cytosolic CaM levels

A major aspect of Ca^{2+}-dependent inactivation is the involvement of CaM which associates with the channel. To investigate the mechanism of APC-induced changes in $I_{Ca,L}$ inactivation kinetics, changes in the expression of cytosolic CaM were determined by Western blot analysis. CaM expression levels were compared between the non-APC and APC groups (n = 6 hearts per group). As shown in Figure 5, the cytosolic CaM expression levels, normalized to β-actin, were unchanged by APC. This suggested that APC did not induce a change in the expression levels of CaM.

Attenuation of cytosolic Ca^{2+} accumulation

Based on our results, *in vivo* APC significantly improved cell survival and also triggered the acceleration of $I_{Ca,L}$ inactivation kinetics that could lead to diminished Ca^{2+} influx. However, the question of whether APC did indeed result in the attenuation of cytosolic Ca^{2+} accumulation in our model still remained. This was addressed by monitoring cytosolic Ca^{2+} with confocal microscopy. Using an identical oxidative stress protocol as in the cell survival study described above, cytosolic Ca^{2+} was monitored by loading isolated myocytes with the fluo-4-AM fluorescent indicator and monitored over time.

Table 1 The effects of *in vivo* APC on the steady-state activation and inactivation curves, and recovery from fast and slow inactivation of $I_{Ca,L}$

	non-APC	*APC*	N *per group*
Steady-state activation			
$V_{1/2}$ (mV)	−16.4 ± 0.6	−17.8 ± 0.9	21–22
k	4.9 ± 0.2	4.6 ± 0.2	
Steady-state inactivation			
$V_{1/2}$ (mV)	−31.0 ± 0.5	−31.7 ± 0.5	22
k	5.1 ± 0.1	4.8 ± 0.1	
Recovery from fast inactivation			
τ (ms)	91.8 ± 3.4	86.7 ± 4.0	19
Recovery from slow inactivation			
τ_{fast} (s)	0.47 ± 0.03	0.42 ± 0.04	4
τ_{slow} (s)	6.4 ± 1.8	6.5 ± 1.1	

Data are presented as mean ± SEM.

Rats in the *in vivo* APC group were exposed to isoflurane prior to thoracotomy as described in *Methods*. As shown in Figure 6, cytosolic Ca^{2+} accumulation was observed in both the non-APC and APC groups following oxidative stress. However, in myocytes isolated from the APC group, this accumulation of Ca^{2+} was significantly attenuated as compared with that of the non-APC group. These results demonstrated that myocytes from the APC group were better protected against stress-induced Ca^{2+} accumulation.

Action potential simulation

To characterize the effects of accelerated $I_{Ca,L}$ inactivation kinetics on the AP, simulations were conducted. Simulations were run using a modified FMG model of the cardiac AP as described in *Methods*. The resultant simulation is depicted in Figure 7A. As expected, the $I_{Ca,L}$ activation and inactivation kinetics during an AP with dynamic changes in the membrane potential differed from those observed during a rectangular test pulse. In the modified FMG model, based on our experimental results, the descending phase of the $I_{Ca,L}$ inactivation was accelerated by 23% in the APC-simulated $I_{Ca,L}$ compared with the control-simulated $I_{Ca,L}$. This change in $I_{Ca,L}$ inactivation kinetics resulted in a limited shortening of the APD, as shown in Figure 7B. In the control-simulated AP, the APD_{50} and APD_{90} were 83.0 and 98.1 ms, respectively, while in the APC-simulated AP, they were 77.8 and 92.9 ms.

Although changes in CaM levels did not appear to account for the accelerated inactivation kinetics based on our Western blot analysis, AP simulations were run to test whether changes in Ca^{2+} sensitivity of the L-type Ca channel can lead to the observed changes in inactivation. To accommodate this change in Ca^{2+} sensitivity, the half-saturation constant for Ca^{2+} in the modified FMG model was adjusted (see *Methods*). We found that arbitrarily decreasing the half-saturation constant by approximately 28%, from 0.60 to 0.43 μmol·L^{-1}, accelerated the inactivation of $I_{Ca,L}$ by only 5% (Figure 8).

Rat strain-dependent effects

Previous studies have reported on rat strain-dependent differences in resistance to myocardial ischaemia, indicative of a genetic component to cardioprotection (Baker *et al.*, 2000). However, rat strain-dependent differences for APC have not been established. We conducted survival studies on cardiomyocytes from the Dahl S strain of rats and found that they showed resistance to the cardioprotective effects of *in vivo* APC (n = 5–9 per group; Figure 9a). This contrasted the effects of APC on the Wistar rats (Figure 1). Subsequently, to confirm that the observed changes in $I_{Ca,L}$ inactivation were correlated with APC, we profiled the $I_{Ca,L}$ inactivation in myocytes isolated from the Dahl S rats. As shown in Figure 9 (panels B and C), APC failed to alter $I_{Ca,L}$ inactivation kinetics in myocytes obtained from the Dahl S rats (n = 9 per group). Thus, in a rat strain that is resistant to APC, changes in $I_{Ca,L}$ inactivation were not evident.

Discussion and conclusions

In the present study, we found that *in vivo* APC by isoflurane accelerated $I_{Ca,L}$ inactivation kinetics, while all other measured biophysical characteristics of the L-type Ca channel remained unchanged. Although the acute inhibitory effects of volatile anaesthetics on the cardiac L-type Ca channel have been previously reported (Bosnjak *et al.*, 1991; Pancrazio, 1996; Camara *et al.*, 2001; Suzuki *et al.*, 2002), this is the first report on an APC-triggered persistent change in a biophysical property of the channel. The voltage-dependent inactivation of the channel was not affected by *in vivo* APC, suggesting that the induced change in inactivation kinetics was due to the effects of APC on Ca^{2+}-dependent inactivation. In addition, these observed changes in $I_{Ca,L}$ inactivation in the Wistar rats were not evident in the Dahl S rats that were resistant to APC. Thus, the changes in $I_{Ca,L}$ inactivation observed in the Wistar rats are a consequence of APC.

The mechanism underlying this observation is unknown. Based on the biophysical analysis, APC induced the L-type Ca channels to favour the fast inactivated state. Key components of Ca^{2+}-dependent inactivation of the L-type Ca channel are modulated by CaM, whereby binding of Ca^{2+} to CaM that is bound to the carboxy-terminal tail of the α-subunit of the channel is a likely necessary step (Peterson *et al.*, 1999; Van Petegem *et al.*, 2005; Zhou *et al.*, 2005). Using a general approach, we hypothesized that APC triggered changes in the CaM levels that can be linked to changes in the L-type Ca channel inactivation. Our results showed that APC did not induce changes in cytosolic CaM levels. Consequently, the accelerated inactivation of $I_{Ca,L}$ was not due to changes in the expression levels of CaM. However, this does not exclude potential changes in the functional role of CaM in the inactivation of $I_{Ca,L}$. For example, changes in the Ca^{2+} binding to the C-lobe of CaM, purported to be a required step for Ca^{2+}-dependent inactivation (Peterson *et al.*, 1999; Alseikhan *et al.*, 2002), can potentially be modified by APC. Additionally, since binding of apoCaM to the IQ motif of the L-type Ca channel is also a critical component of inactivation (Tang *et al.*, 2003), changes in this interaction could also influence Ca^{2+}-dependent inactivation.

Although the net physiological consequence of the APC-triggered change in $I_{Ca,L}$ inactivation was not established, it

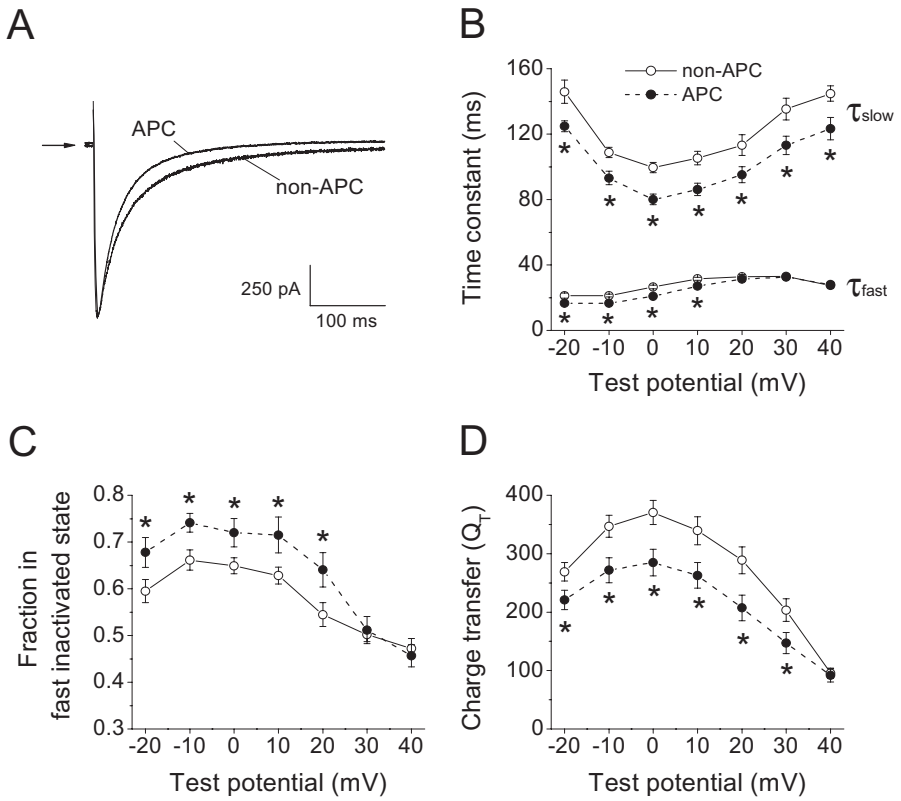

Figure 3 Effects of *in vivo* APC on voltage- and Ca^{2+}-dependent inactivation of the cardiac L-type Ca channel. (A) Sample whole-cell $I_{Ca,L}$ traces recorded from myocytes in the non-APC and APC groups monitored at 0 mV from a holding potential of −80 mV are shown. The current traces were superimposed. Arrow indicates zero current level. (B) The fast and slow time constants of the inactivation kinetics of $I_{Ca,L}$ in myocytes from the non-APC and APC groups are plotted against test potentials. Compared with the non-APC group, APC significantly decreased τ_{fast} in the range from −20 to +10 mV and τ_{slow} in the range from −20 to +40 mV. (C) The fraction of channels that 'fast inactivated' was determined from the double exponential fit to the inactivating $I_{Ca,L}$ traces. In the APC group, the fraction in the fast inactivated state was significantly increased compared to the non-APC group. (D) Changes in $I_{Ca,L}$ inactivation was correlated to changes in the total influx of charge by integrating the area of $I_{Ca,L}$ traces during a 100 ms period. The charge transfer was significantly decreased by APC in the range from −20 to +30 mV. $^*P < 0.05$ vs. non-APC. $n = 21–22$ per group.

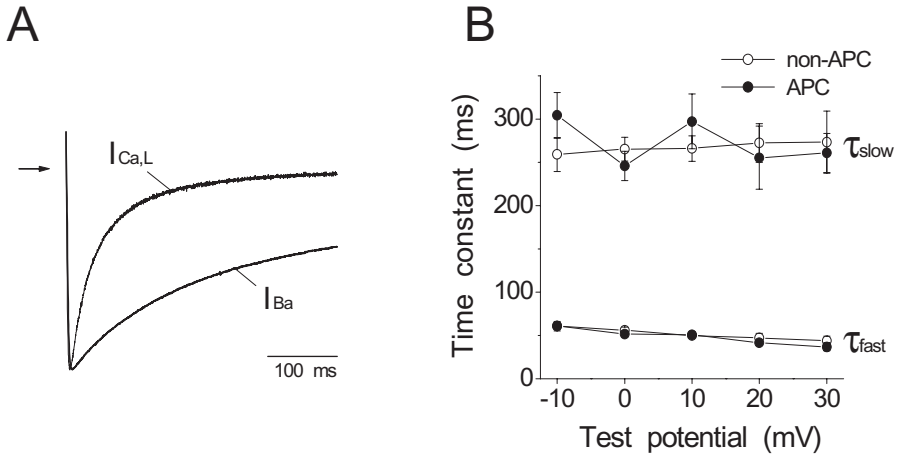

Figure 4 Effects of *in vivo* APC on the voltage-dependent inactivation of the cardiac L-type Ca channel. (A) Representative traces of $I_{Ca,L}$ and I_{Ba} recorded at 0 mV from a holding potential of −80 mV using Ca^{2+} and Ba^{2+} as charge carriers, respectively, are shown. The currents were scaled and superimposed. Arrow indicates zero current level. Ba^{2+} as the charge carrier removed Ca^{2+}-dependent inactivation of the L-type Ca channel. (B) The fast and slow time constants of the inactivation kinetics of I_{Ba} in the non-APC and APC groups are plotted against test potentials. No significant differences were observed in τ_{fast} and τ_{slow} between the non-APC and APC groups ($n = 10$ per group).

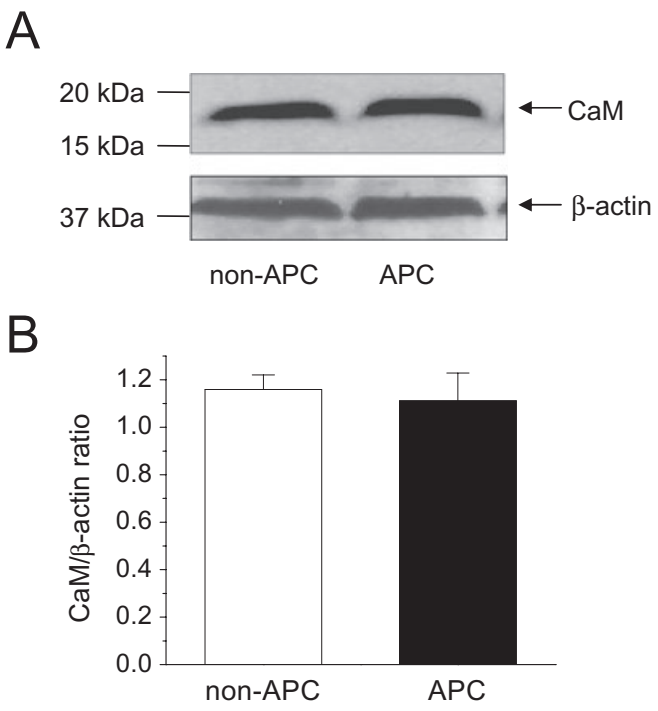

Figure 5 Cytosolic calmodulin (CaM) levels. Effects of *in vivo* APC on cytosolic CaM levels were determined by Western blot. (A) Representative results from one heart each from the non-APC and APC groups are shown. β-actin was used as the loading control. (B) Summary of the CaM/β-actin ratio in the non-APC and APC groups are shown. No significant differences were observed between two groups ($n = 6$ hearts per group).

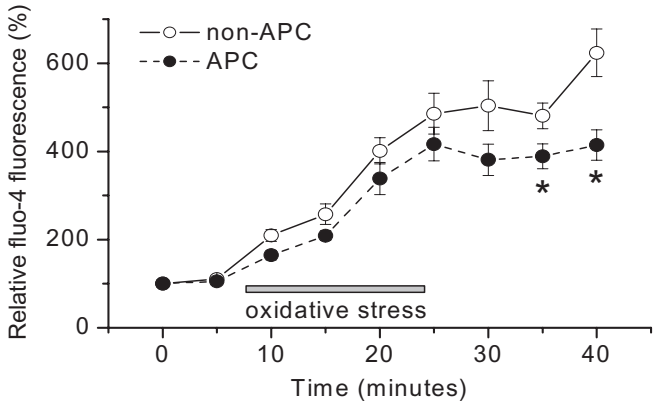

Figure 6 Cytosolic Ca^{2+} accumulation under stress conditions. Isolated cardiomyocytes were loaded with the cytosolic Ca^{2+} indicator, fluo-4-AM, and exposed to oxidative stress, followed by perfusion with glucose-free Tyrode solution. Fluo-4 fluorescence was monitored over time. Myocytes from both the non-APC and APC groups showed increases in cytosolic Ca^{2+} following stress as indicated by the increases in fluo-4 fluorescence. However, the increase in fluo-4 fluorescence was significantly reduced in the APC-treated myocytes. *$P < 0.05$ vs. non-APC. $n = 10$–12 per group.

can potentially contribute to reduced Ca^{2+} influx and to changes in cardiac electrophysiology. Regarding the former, since the L-type Ca channel is a major route of Ca^{2+} influx into the cytosol, the acceleration of $I_{Ca,L}$ inactivation kinetics can potentially contribute to a decrease in Ca^{2+} overload, and

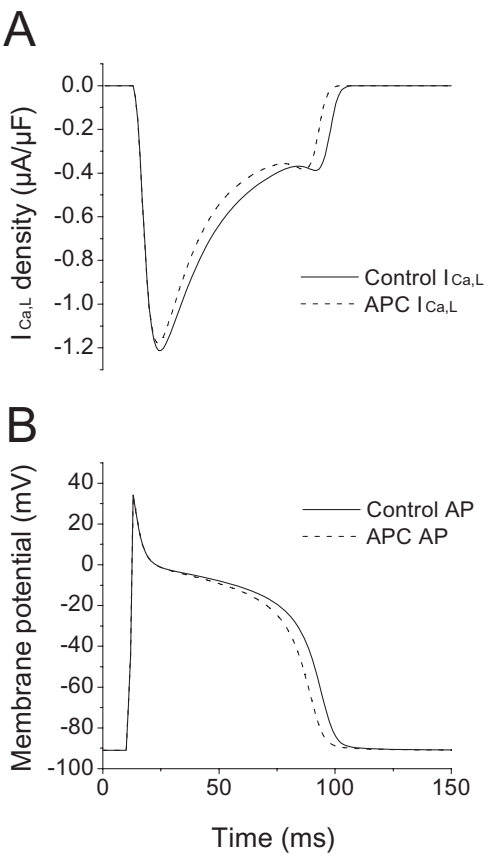

Figure 7 Simulation of the action potential. (A) Using a modified FMG model as described in *Methods*, inactivation kinetics were accelerated by 23% in the simulated APC $I_{Ca,L}$ compared with the Control $I_{Ca,L}$. (B) Simulated changes in the AP (control vs. APC) are shown as the corresponding consequence of the accelerated $I_{Ca,L}$ inactivation. The APD_{50} and APD_{90} were 83.0 and 98.1 ms, respectively, in the control-simulated AP, and 77.8 and 92.9 ms in the APC-simulated AP.

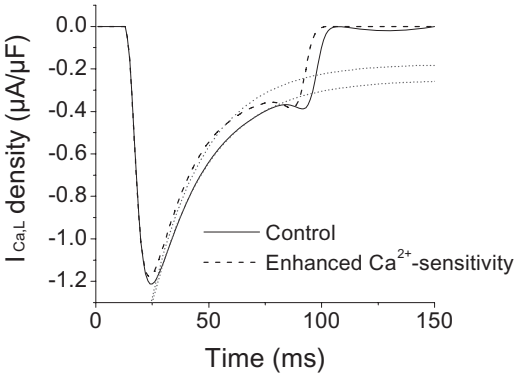

Figure 8 Effect of Ca^{2+} sensitivity on $I_{Ca,L}$ inactivation. The effect of altering the sensitivity of L-type Ca channels to intracellular Ca^{2+} on $I_{Ca,L}$ inactivation was simulated using the modified FMG model. Ca^{2+} sensitivity was enhanced by 28% (dashed lines) relative to the control. The exponential fits are depicted by the dotted lines. This enhancement of Ca^{2+} sensitivity induced only 5% change in the acceleration of the $I_{Ca,L}$ inactivation.

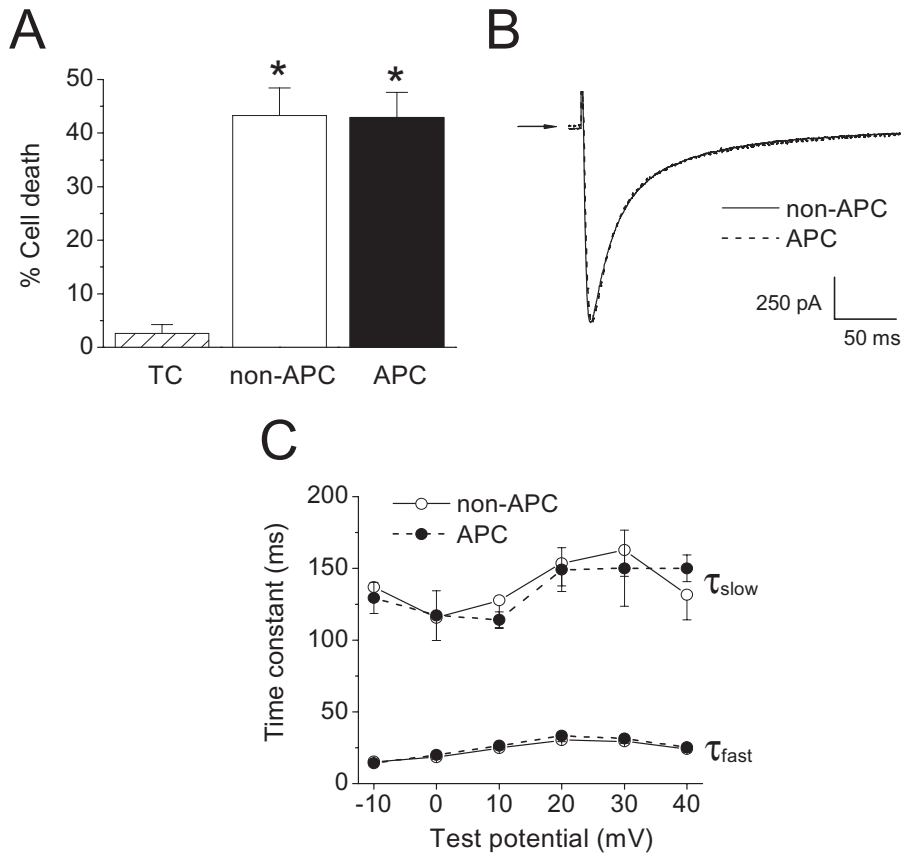

Figure 9 Effects of *in vivo* APC on the Dahl S strain of rats. (A) Cell survival study. Oxidative stress significantly increased the percentage of cell death in the non-APC group compared with the time control (TC) group. In the APC group, cell survival following oxidative stress was not significantly different from the APC group, indicating resistance to cardioprotection in the Dahl S rats. *$P < 0.05$ vs. TC. $n = 5$–9 per group. (B) Representative whole-cell $I_{Ca,L}$ traces from Dahl S myocytes in the non-APC and APC groups. Currents were recorded at a test potential of 0 mV from a holding potential of −80 mV. The traces shown were superimposed. Arrow indicates zero current level. (C) $I_{Ca,L}$ inactivation kinetics. The fast and slow time constants of current inactivation in myocytes from the non-APC and APC groups showed no significant differences in the Dahl S rats ($n = 9$ per group).

subsequently reduce mitochondrial Ca^{2+} overload, and prevent or delay apoptosis. Our results showed a significant decrease in the total charge transfer as a result of the accelerated $I_{Ca,L}$ inactivation by APC. Studies have indeed demonstrated that APC significantly reduced cytosolic Ca^{2+} concentration, relative to non-preconditioned hearts following global ischaemia (An *et al.*, 2001; Varadarajan *et al.*, 2002), and attenuated cytochrome c release from mitochondria (Qian *et al.*, 2005). These effects can be correlated with a reduction in infarct size and with improved functional recovery following ischaemia/reperfusion.

In addition to the L-type Ca channel, contributions from other sources of Ca^{2+}, for example, the roles of the Na^+/Ca^{2+} exchanger and the ryanodine receptors on the sarcoplasmic reticulum, and the buffering capacity of the mitochondria, must also be considered in determining the precise mechanism(s) underlying Ca^{2+} overload attenuation, induced by APC. Our results showed that cytosolic Ca^{2+} accumulation was decreased following oxidative stress in myocytes obtained from preconditioned hearts. Although this demonstrated the functional efficacy of our APC model, the contribution from the L-type Ca channel in attenuating Ca^{2+} overload was uncertain as the Ca^{2+} measurements were conducted under *in vitro* conditions in non-contracting myocytes. Consequently, other mechanisms are likely to be involved. On the other hand, in a beating heart, cytosolic Ca^{2+} accumulation following stress might be greater due to influx of Ca^{2+} via the L-type Ca channel, which is a major source of Ca^{2+} entry into the cytosol. Thus, one can speculate that the acceleration of $I_{Ca,L}$ inactivation kinetics triggered by APC would be likely to contribute to decreased Ca^{2+} accumulation in contracting myocytes. Overall, our results suggested that the preconditioned myocytes were better able to handle Ca^{2+} accumulation following stress.

With regard to cardiac electrophysiology, though the cardioprotective effect of APC is well established, in terms of reduction in infarct size, its effect against arrhythmias has not been firmly documented. For example, studies using the isolated heart model of APC showed that sevoflurane can delay the onset of ventricular fibrillation or have no effect on this type of arrhythmia (Novalija *et al.*, 1999; Kevin *et al.*, 2003). Based on our simulation studies, the accelerated $I_{Ca,L}$ inactivation would result in the shortening of the cardiac APD. It is well established that APC enhances the opening of the $sarcK_{ATP}$ channel and this effect can also lead to the shortening of the APD. Consequently, the acceleration of $I_{Ca,L}$ inactivation could

potentiate this effect, resulting in a further shortening of the APD and triggering re-entrant arrhythmias. Hence, a critical balance between the sarcK_{ATP} channel opening and acceleration of $I_{Ca,L}$ inactivation may underlie some of the confusion regarding the effects of APC on cardiac rhythm. The overall effect on cardiac electrophysiology, thus, will depend on the cumulative effects the APC-triggered signalling cascade would have on the various sarcolemmal ion channels. Furthermore, it may also depend on the timing of the opening of the sarcK_{ATP} channel. Currently, the magnitude and duration of the activation of the sarcK_{ATP} channel during the various phases of preconditioning (stimulus, washout, ischaemia and reperfusion) are unknown, although a recent study suggested that the sarcK_{ATP} channels were more likely to open during the ischaemia/reperfusion period and contribute to cardioprotection (Marinovic *et al.*, 2006; Stadnicka *et al.*, 2006).

One intriguing but remarkable aspect of our findings is that only one biophysical characteristic of the L-type Ca channel, the rate of inactivation, was affected by APC. All other measured parameters remained unchanged. The direct, acute application of volatile anaesthetics is known to inhibit $I_{Ca,L}$ amplitude and thus to depress cardiac contractility (Hanley *et al.*, 2004). However, this inhibition is absent in the persistent effect triggered by isoflurane preconditioning. This change in the inactivation kinetics may allow for the fine tuning of Ca^{2+} entry without affecting the contractile ability of the cardiac myocytes. Furthermore, a recent study proposed that accelerating $I_{Ca,L}$ inactivation while preserving peak $I_{Ca,L}$ may be an effective way to prevent arrhythmias (Mahajan *et al.*, 2008).

To date, studies systematically exploring the effect of APC on the cardiac sarcolemmal voltage-gated ion channels have been limited, despite the strong probability that the signalling mechanism triggered by APC can modulate the function of these proteins. In pursuit of the mechanism underlying APC, studies have focused on the intracellular signalling cascade and on mitochondrial function (Bienengraeber *et al.*, 2005). With respect to the role of ion channels in APC, those not gated by voltage, specifically the sarcK_{ATP} and mitoK_{ATP} channels, have been intensely investigated. The roles of other ion channels, particularly those on the mitochondria such as the voltage-dependent anion and the calcium activated potassium channels and the adenine nucleotide translocase, have yet to be established.

In conclusion, the results of this study showed that *in vivo* APC triggered the acceleration of $I_{Ca,L}$ inactivation kinetics in cardiomyocytes. Voltage-dependent inactivation of $I_{Ca,L}$ was not affected, suggesting the involvement of Ca^{2+}-dependent inactivation. Although a direct physiological consequence of this change in inactivation has yet to be determined, this alteration in the L-type Ca channel may contribute to the preservation of cardiomyocytes against Ca^{2+} overload and subsequent cell death.

Acknowledgements

This work was supported by grant No. PO1 GM066730 (Project III to WMK; Program Director ZJB) from the National Institutes of Health, Bethesda, MD, USA. The authors thank Dr Martin W. Bienengraeber (Assistant Professor, Departments of Anesthesiology and Pharmacology and Toxicology, Medical College of Wisconsin, Milwaukee, WI, USA), and Dr Garrett J. Gross (Professor, Department of Pharmacology and Toxicology, Medical College of Wisconsin, Milwaukee, WI, USA) for valuable discussions.

Conflicts of interest

None.

References

Aizawa K, Turner LA, Weihrauch D, Bosnjak ZJ, Kwok WM (2004). Protein kinase C-epsilon primes the cardiac sarcolemmal adenosine triphosphate-sensitive potassium channel to modulation by isoflurane. *Anesthesiology* **101**: 381–389.

Alseikhan BA, DeMaria CD, Colecraft HM, Yue DT (2002). Engineered calmodulins reveal the unexpected eminence of Ca2+ channel inactivation in controlling heart excitation. *Proc Natl Acad Sci USA* **99**: 17185–17190.

An J, Varadarajan SG, Novalija E, Stowe DF (2001). Ischemic and anesthetic preconditioning reduces cytosolic [Ca2+] and improves Ca(2+) responses in intact hearts. *Am J Physiol Heart Circ Physiol* **281**: H1508–H1523.

Baker JE, Konorev EA, Gross GJ, Chilian WM, Jacob HJ (2000). Resistance to myocardial ischemia in five rat strains: is there a genetic component of cardioprotection? *Am J Physiol Heart Circ Physiol* **278**: H1395–H1400.

Bienengraeber MW, Weihrauch D, Kersten JR, Pagel PS, Warltier DC (2005). Cardioprotection by volatile anesthetics. *Vascul Pharmacol* **42**: 243–252.

Bosnjak ZJ, Supan FD, Rusch NJ (1991). The effects of halothane, enflurane, and isoflurane on calcium current in isolated canine ventricular cells. *Anesthesiology* **74**: 340–345.

Cain BS, Meldrum DR, Cleveland JC Jr, Meng X, Banerjee A, Harken AH (1999). Clinical L-type Ca(2+) channel blockade prevents ischemic preconditioning of human myocardium. *J Mol Cell Cardiol* **31**: 2191–2197.

Camara AK, Begic Z, Kwok WM, Bosnjak ZJ (2001). Differential modulation of the cardiac L- and T-type calcium channel currents by isoflurane. *Anesthesiology* **95**: 515–524.

Cason BA, Gamperl AK, Slocum RE, Hickey RF (1997). Anesthetic-induced preconditioning: previous administration of isoflurane decreases myocardial infarct size in rabbits. *Anesthesiology* **87**: 1182–1190.

Dick IE, Tadross MR, Liang H, Tay LH, Yang W, Yue DT (2008). A modular switch for spatial Ca2+ selectivity in the calmodulin regulation of CaV channels. *Nature* **451**: 830–834.

Findlay I (2002). Voltage-dependent inactivation of L-type Ca2+ currents in guinea-pig ventricular myocytes. *J Physiol* **545**: 389–397.

Fox JJ, McHarg JL, Gilmour RF Jr (2002). Ionic mechanism of electrical alternans. *Am J Physiol Heart Circ Physiol* **282**: H516–H530.

Galinanes M, Hearse DJ (1990). Species differences in susceptibility to ischemic injury and responsiveness to myocardial protection. *Cardioscience* **2**: 127–143.

Garny A, Kohl P, Noble D (2003). Cellular Open Resource (COR): a public CellML based environment for modelling biological function. *Int J Bifurcat Chaos* **13**: 3579–3590.

Hanley PJ, ter Keurs HE, Cannell MB (2004). Excitation-contraction coupling in the heart and the negative inotropic action of volatile anesthetics. *Anesthesiology* **101**: 999–1014.

Hoka S, Bosnjak ZJ, Kampine JP (1987). Halothane inhibits calcium accumulation following myocardial ischemia and calcium paradox in guinea pig hearts. *Anesthesiology* **67**: 197–202.

Kersten JR, Schmeling TJ, Pagel PS, Gross GJ, Warltier DC (1997a). Isoflurane mimics ischemic preconditioning via activation of K(ATP) channels: reduction of myocardial infarct size with an acute memory phase. *Anesthesiology* **87**: 361–370.

Kersten JR, Orth KG, Pagel PS, Mei DA, Gross GJ, Warltier DC (1997b). Role of adenosine in isoflurane-induced cardioprotection. *Anesthesiology* **86**: 1128–1139.

Kevin LG, Katz P, Camara AK, Novalija E, Riess ML, Stowe DF (2003). Anesthetic preconditioning: effects on latency to ischemic injury in isolated hearts. *Anesthesiology* **99**: 385–391.

Krolikowski JG, Bienengraeber M, Weihrauch D, Warltier DC, Kersten JR, Pagel PS (2005). Inhibition of mitochondrial permeability transition enhances isoflurane-induced cardioprotection during early reperfusion: the role of mitochondrial KATP channels. *Anesth Analg* **101**: 1590–1596.

Linz KW, Meyer R (2000). Profile and kinetics of L-type calcium current during the cardiac ventricular action potential compared in guinea-pigs, rats and rabbits. *Pflugers Arch* **439**: 588–599.

Ljubkovic M, Mio Y, Marinovic J, Stadnicka A, Warltier DC, Bosnjak ZJ *et al*. (2007). Isoflurane preconditioning uncouples mitochondria and protects against hypoxia-reoxygenation. *Am J Physiol Cell Physiol* **292**: C1583–C1590.

Ludwig LM, Weihrauch D, Kersten JR, Pagel PS, Warltier DC (2004). Protein kinase C translocation and Src protein tyrosine kinase activation mediate isoflurane-induced preconditioning in vivo: potential downstream targets of mitochondrial adenosine triphosphate-sensitive potassium channels and reactive oxygen species. *Anesthesiology* **100**: 532–539.

Luo CH, Rudy Y (1994). A dynamic model of the cardiac ventricular action potential. I. Simulations of ionic currents and concentration changes. *Circ Res* **74**: 1071–1096.

Mahajan A, Sato D, Shiferaw Y, Baher A, Xie LH, Peralta R *et al*. (2008). Modifying L-type calcium current kinetics: consequences for cardiac excitation and arrhythmia dynamics. *Biophys J* **94**: 411–423.

Marinovic J, Bosnjak ZJ, Stadnicka A (2006). Distinct roles for sarcolemmal and mitochondrial adenosine triphosphate-sensitive potassium channels in isoflurane-induced protection against oxidative stress. *Anesthesiology* **105**: 98–104.

Miyawaki H, Ashraf M (1997). Ca2+ as a mediator of ischemic preconditioning. *Circ Res* **80**: 790–799.

Murry CE, Jennings RB, Reimer KA (1986). Preconditioning with ischemia: a delay of lethal cell injury in ischemic myocardium. *Circulation* **74**: 1124–1136.

Novalija E, Fujita S, Kampine JP, Stowe DF (1999). Sevoflurane mimics ischemic preconditioning effects on coronary flow and nitric oxide release in isolated hearts. *Anesthesiology* **91**: 701–712.

Pancrazio JJ (1996). Halothane and isoflurane preferentially depress a slowly inactivating component of Ca2+ channel current in guinea-pig myocytes. *J Physiol* **494**: 91–103.

Peterson BZ, DeMaria CD, Adelman JP, Yue DT (1999). Calmodulin is the Ca2+ sensor for Ca2+ -dependent inactivation of L-type calcium channels. *Neuron* **22**: 549–558.

Qian LP, Zhu SS, Cao JL, Zeng YM (2005). Isoflurane preconditioning protects against ischemia-reperfusion injury partly by attenuating cytochrome c release from subsarcolemmal mitochondria in isolated rat hearts. *Acta Pharmacol Sin* **26**: 813–820.

Riess ML, Kevin LG, McCormick J, Jiang MT, Rhodes SS, Stowe DF (2005). Anesthetic preconditioning: the role of free radicals in sevoflurane-induced attenuation of mitochondrial electron transport in Guinea pig isolated hearts. *Anesth Analg* **100**: 46–53.

da Silva R, Grampp T, Pasch T, Schaub MC, Zaugg M (2004). Differential activation of mitogen-activated protein kinases in ischemic and anesthetic preconditioning. *Anesthesiology* **100**: 59–69.

Smith GB, Stefenelli T, Wu ST, Wikman-Coffelt J, Parmley WW, Zaugg CE (1996). Rapid adaptation of myocardial calcium homeostasis to short episodes of ischemia in isolated rat hearts. *Am Heart J* **131**: 1106–1112.

Stadnicka A, Marinovic J, Bienengraeber M, Bosnjak ZJ (2006). Impact of in vivo preconditioning by isoflurane on adenosine triphosphate-sensitive potassium channels in the rat heart: lasting modulation of nucleotide sensitivity during early memory period. *Anesthesiology* **104**: 503–510.

Suzuki A, Aizawa K, Gassmayr S, Bosnjak ZJ, Kwok WM (2002). Biphasic effects of isoflurane on the cardiac action potential: an ionic basis for anesthetic-induced changes in cardiac electrophysiology. *Anesthesiology* **97**: 1209–1217.

Tanaka K, Weihrauch D, Kehl F, Ludwig LM, LaDisa JF Jr, Kersten JR *et al*. (2002). Mechanism of preconditioning by isoflurane in rabbits: a direct role for reactive oxygen species. *Anesthesiology* **97**: 1485–1490.

Tang W, Halling DB, Black DJ, Pate P, Zhang JZ, Pedersen S *et al*. (2003). Apocalmodulin and Ca2+ calmodulin-binding sites on the CaV1.2 channel. *Biophys J* **85**: 1538–1547.

Van Petegem F, Chatelain FC, Minor DL Jr (2005). Insights into voltage-gated calcium channel regulation from the structure of the CaV1.2 IQ domain-Ca2+/calmodulin complex. *Nat Struct Mol Biol* **12**: 1108–1115.

Varadarajan SG, An J, Novalija E, Stowe DF (2002). Sevoflurane before or after ischemia improves contractile and metabolic function while reducing myoplasmic Ca(2+) loading in intact hearts. *Anesthesiology* **96**: 125–133.

Zaugg M, Lucchinetti E, Spahn DR, Pasch T, Schaub MC (2002). Volatile anesthetics mimic cardiac preconditioning by priming the activation of mitochondrial K(ATP) channels via multiple signaling pathways. *Anesthesiology* **97**: 4–14.

Zhou H, Yu K, McCoy KL, Lee A (2005). Molecular mechanism for divergent regulation of Cav1.2 Ca2+ channels by calmodulin and Ca2+-binding protein-1. *J Biol Chem* **280**: 29612–29619.